
Evaluating Sparse Galaxy Simulations via Out-of-Distribution Detection and Amortized Bayesian Model Comparison

Lingyi Zhou¹, Stefan T. Radev², William H. Oliver¹, Aura Obreja¹, Zehao Jin³, Tobias Buck¹

¹Interdisciplinary Center for Scientific Computing, Heidelberg University, D-69120 Heidelberg

²Center for Modeling, Simulation, & Imaging in Medicine, Rensselaer Polytechnic Institute, NY, USA

³Center for Astrophysics and Space Science (CASS), New York University Abu Dhabi

Abstract

Cosmological simulations are a powerful tool to advance our understanding of galaxy formation and many simulations model key properties of real galaxies. A question that naturally arises for such simulations in light of high-quality observational data is: How close are the models to reality? Due to the high-dimensionality of the problem, many previous studies evaluate galaxy simulations using simplified summary statistics of physical properties. In this work, we combine simulation-based Bayesian model comparison with a novel misspecification detection technique to compare simulated galaxy images of 6 hydrodynamical models against real Sloan Digital Sky Survey (SDSS) observations. Since cosmological simulations are computationally costly, we address the problem of low simulation budgets by first training a k -sparse variational autoencoder (VAE) on the abundant dataset of SDSS images. The VAE learns to extract informative latent embeddings and delineates the typical set of real images. To reveal simulation gaps, we then perform out-of-distribution (OOD) detection based on the logits of classifiers trained on the embeddings of simulated images. Finally, we perform amortized Bayesian model comparison using probabilistic classification, identifying the relatively best-performing model along with partial explanations through SHAP values.

1 Motivation and related work

Investigating the physical processes that govern the formation and evolution of galaxies is a hard problem. Many of these processes, which span a very large dynamical range, are coupled, and thus, understanding their importance for galaxy formation requires running cosmological hydrodynamical simulations [46]. However, assessing the quality and realism of these simulations is a notoriously difficult task. A common approach is to compare the distribution of galaxy properties retrieved from simulations and observations as a diagnostic tool. However, galaxy observations span a multi-dimensional, complex parameter space (image-like or time series-like data), and it is not clear how to optimally perform model comparison in such a setup. Many previous works have measured the gap between simulation models and observations using traditional methods employing simple 2d or 3d summary statistics, for example, the Tully-Fisher [43] or the stellar mass-halo mass relation [29]. Many modern studies try to match multiple observed properties of galaxies. For instance, UniverseMachine [2], a state-of-the-art algorithm for predicting observable galaxy properties based on simulations, is optimized to simultaneously match a wide range of these properties. However, this is a very limited criterion, as a model may closely match real observations under one such relation, but deviate significantly from reality under another. Recently, several works have explored machine learning approaches to compare simulations and observations. [15] used the deep learning method for Bayesian model comparison proposed by [11] to compare simulation-based supernova Ia light curve models. [50] compared Illustris [45] and IllustrisTNG [34] with r -band Sloan Digital Sky

Survey [SDSS 18] images by combining the output of two PixelCNN networks [44] to produce pixel-wise anomaly scores assigned to simulation images. [14] proposed to use GANomaly [1], an anomaly detection network based on Generative Adversarial Networks [GAN 13], to rate NIHAO simulations [Numerical Investigation of Hundred Astrophysical Objects 4, 5, 47] against SDSS images by assigning anomaly scores to galaxy images. Since galaxy simulations are computationally expensive to obtain ($\sim 10 - 100$ k CPUh per instance), we take a novel approach. We leverage a large set of real images (643,553) to pre-train a sparse embedding network which compresses simulated and real galaxy images into a structured latent space, which allows us to highlight notable simulation gaps [41]. Then, we use the amortized Bayesian model comparison (BMC) [37, 38], which is a novel simulation-based inference [SBI; 9] method for comparing analytically intractable, high-dimensional models, to determine the relative fit of each model. This allows us to efficiently handle a large number of images, which would be computationally infeasible with standard Bayesian methods. Given the limited size of our simulation dataset—an inherent challenge for SBI applications that typically require large amounts of data—we utilize ensemble methods to enhance classifier performance and robustness despite the data scarcity.

2 Datasets and Simulation Details

Observed galaxy images The Sloan Digital Sky Survey [SDSS 7, 18] is one of the most influential astronomical surveys ever conducted. Its main goal is to create detailed multi-dimensional maps of the universe, capturing images and spectra of millions of celestial objects. SDSS images are produced in a set of broad-band filters, of which we use three: the near-infrared (i), red (r), and green (g) which can then be combined into multi-color images by mapping the i, r, g -bands to red, green and blue color channels. Following the work of [14], we use the galaxy catalogue by [28] with redshift from 0.005 to 0.395 (mean of 0.109), and only use galaxies with stellar mass greater than $10^9 M_\odot$ which leaves us with 643,553 galaxy images. For training our embedding network, we split SDSS into a training (70%), a test (10%) and two validation sets: one for early stopping (10%) and one for hyperparameter tuning (10%).

Simulated galaxy images We compare simulated galaxy images from six candidate models taken from two different simulation projects: TNG50 and TNG100 from the IllustrisTNG simulations [31–33, 35, 42] and AGN [3, 48], NOAGN [47], UHD [Ultra High Definition 5] and n80 [23] from the NIHAO simulation suite. The only difference between TNG100 and TNG50 is the physical resolution of the underlying simulation, while in the case of NIHAO the different flavours explore different physical models for star formation and feedback in addition to increased resolution. More information on the exact differences between the various simulation flavours of NIHAO can be found in [14]. All simulated galaxy images are created with the same image pipeline based on radiative transfer (RT) post-processing of the simulated galaxies using the SKIRT code [6]. For the IllustrisTNG models we use the synthetic image data from [40], available on the open data access website¹. For the NIHAO models we use the synthetic data from [14]. For both simulation projects, we create RGB images from the raw RT output following the image pipeline of [14] which combines the i, r, g images using an arcsinh stretch as proposed by [22] and we add observational realism including point spread function (PSF) convolution, shot noise, and Gaussian sky noise. We adopt a Gaussian PSF with full width at half-maximum (FWHM) at the average seeing of all SDSS Legacy galaxies (1.286'', 1.356'', and 1.496'' for SDSS $i - r - g$ bands). The physical width of the simulated galaxies is converted to angular size by hypothetically putting them at a distance of redshift $z = 0.109$, the mean redshift of our SDSS training sample. The shot noise is taken as Poisson noise determined by zeropoints, airmass, extinction, and CCD gain in the survey fields. Gaussian sky noise is obtained from the average sky noise over all Legacy galaxies.

In the following figures, NIHAO models are named with an additional suffix “rt” to distinguish them from a previous version of our image data. Our final simulated image dataset has a resolution of 64x64 pixels and includes 11334, 1523, 1521, 1540, 120, and 240 images for TNG100, TNG50, AGN, NOAGN, UHD, and n80, respectively. Because the simulation dataset is imbalanced (TNG100 is the majority class), we oversample the images in the minority classes by copying them once. In our experiments, without oversampling, the classifiers in later steps are poorly calibrated with

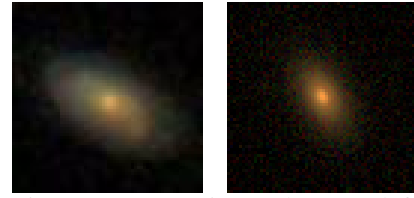


Figure 1: Comparing real SDSS (left) and simulated NOAGN (right) galaxies.

¹<https://www.tng-project.org/data/docs/specifications/#sec51>

suboptimal confusion matrices and calibration curves. For the subsequent steps of model comparison, we stratify the latent embeddings of the simulation models into a training set (85%) and a test set (15%), ensuring that the class proportions remain unchanged after the split. We perform train-test split before oversampling so that copies do not get split across training and test sets.

3 Method

Learning summary statistics with limited simulation budgets A typical approach in SBI methods for model comparison is reducing the original data into fixed summary statistics (also called latent embeddings in our context) to avoid working with high-dimensional observables, such as galaxy images. Additionally, [37] proposed to train embedding networks that capture the structure of the original data, avoiding catastrophic information loss and biased results caused by hand-crafted summary statistics [26, 39]. However, learning summary statistics end-to-end requires large simulation budgets that are infeasible in our setting. For instance, running the TNG100 simulations alone on Cray XC40 Hazel Hen supercomputer² demands 1.5 years of runtime, equivalent to millions of CPU hours, making such simulation efforts prohibitively expensive. To overcome this problem, we leverage the large body of real observational data from SDSS to train an embedding network (i.e., an encoder) in a fully unsupervised manner as part of an information maximizing variational autoencoder architecture. Then, we “freeze” the encoder and embed the simulated images into the lower dimensional latent space. This smaller subset of “labeled” embeddings serves as the training data for an ensemble of classifiers that learns to perform Bayesian model comparison and detect simulation gaps.

Auto-encoding galaxy images We use a k -sparse variational autoencoder [VAE; 17] based on the k -sparse autoencoder [25] to encode galaxy images to latent embeddings since compared to plain autoencoders, VAEs provide a probabilistic framework and help prevent overfitting. To this end, we compute embeddings z using the reparameterization trick and we incorporate the Maximum Mean Discrepancy (MMD) VAE loss from the InfoVAE family [51] to avoid common problems with the standard VAE model and encourage maximally informative compression. Our final loss function is $\mathcal{L} = \text{MMD}^2(q_\phi(z)\|p(z)) + \text{MSE}(x_{\text{recon}}, x)$ where $p(z) \sim \mathcal{N}(0, I)$, $q_\phi(z)$ denotes the approximate distribution of the embedding z , MSE stands for mean squared error, x is the image and x_{recon} is the image reconstructed by the decoder. During training, we compute the latent embedding z in the feedforward phase, then sparsify it by keeping only the k largest activations (absolute values) and setting the rest to zero. The computation of the loss function and the input of the decoder both use the sparsified z . We train the k -sparse VAE on the SDSS training set with dimension $z = 512$ and $k = 32$. We choose the sparsity ratio to be $32/512 = 0.0625$ for our k -sparse VAE achieving a balance between capturing local features and global features [25]. Then we encode the SDSS test set and the simulated images to 512 dimensional latent embeddings with $k = 64$. A larger k during the encoding phase reduces the error rate of downstream classification task [25]. Different k values for training and testing do not introduce any systematic effects that could resemble OOD behavior; otherwise, the classifier’s performance would worsen as it would not handle OOD data well.

Amortized Bayesian model comparison and misspecification detection Bayesian model comparison (BMC) offers a relative comparison of multiple models rather than an absolute assessment of any individual model. It can be cast into a classification task by training a classifier with a strictly proper loss [12] to induce a categorical distribution over the model indices \mathcal{M} given the observed data D : $\mathcal{M} \sim p(\mathcal{M} | D)$ [37]. Correspondingly, we train an ensemble of classifiers on the “labeled” latent embeddings of the simulated images and then use the trained ensemble to estimate posterior model probabilities from the SDSS test set in an instant. The model with the best relative fit from a Bayesian perspective [24, 37] is then the one that is preferred by the classifier. The classifier can be efficiently reused for inference as new observations come in - hence the training cost *amortizes* over multiple observations. However, we cannot simply apply the ensemble to all latent embeddings of our SDSS test set since some of them may be out-of-distribution [OOD; 49] relative to the simulations, which can lead to incorrect or unstable predictions [10, 41]. In our context, OOD occurs when the simulations differ significantly from the (actually observed) test data and thus indicates model misspecification. We can use any *post hoc* OOD score [49] to *detect* observations for which the models are misspecified. A *post hoc* OOD score identifies OOD samples using a trained model’s outputs without retraining or altering the model. We perform out-of-distribution (OOD) detection using the Generalized ENtropy score [GEN score 19] which is defined as $G_\gamma(p) = \sum_j p_j^\gamma (1 - p_j)^\gamma$

²<https://www.tng-project.org/people/>

with $\gamma \in (0, 1)$, where p are the probabilities of all classes calculated by applying the softmax function to the logits produced by the classifiers. In practice, we set $\gamma = 0.1$ and following the original paper [19], we compute negative GEN scores. In order to perform OOD detection, we proceed as follows: We fit a classifier to the SDSS test set and compute the corresponding GEN score distribution. Similarly, we compute the reference GEN score distribution by classifying the simulation test sets. If the GEN score distribution of SDSS test set lies significantly outside of the reference GEN score distribution, then the SDSS test set is OOD, implying that the simulations deviate from reality. In this case, we perform model comparison only on the subset of SDSS data that “agree” with simulated latent embeddings. For this, we take the percent point corresponding to 95% of the reference GEN score distribution as a threshold and ignore all SDSS latent embeddings with a GEN score beyond this threshold. To this “cleaned” SDSS test dataset we apply the classifiers once again to derive our final model posteriors. In this way, we can increase the robustness of model posterior estimates and the corresponding theoretical implications.

Classifiers and training objectives Our baseline model is a random forest classifier, also used in previous model comparison papers [26, 36] and we further train a XGBoost model [8]. As stated before, we have a small set of simulation data and ensemble methods handle this situation better than a single neural network. So we additionally train a stacking ensemble classifier (stacking-MLP-RF-XGB), which combines 3 base classifiers (MLP, random forest and XGBoost) with a random forest serving as the final estimator. Before we train the final classifiers on the simulation models, we use 5-fold cross validation to select the best classifier using the calibration curve (Figure 5) and confusion matrix (Figure 6) as metric. The derived expected calibration error score [ECE score 30] and the confusion matrices show that the stacking-MLP-RF-XGB classifier achieves better recovery than random forest or XGBoost.

4 Results

UMAP visualization of latent embeddings We visualize the latent space embedding using UMAP [Uniform Manifold Approximation and Projection, 27] to project the 512-d latent embeddings into a 2-d space in Figure 2. We train the UMAP model solely on the SDSS test set to obtain the corresponding embeddings and apply it then to each simulation to visualize the relative positions of simulated data and SDSS test set.

By doing so we can get an intuition of the gap between the simulation models and reality. It is clear that the latent embeddings from the 6 simulation models overlap only with a small part of the SDSS test data which implies that all simulation models can only explain a small fraction of observed galaxies. This is further confirmed by the GEN score distributions which are generally of different shape for the observational dataset and the simulation models (Figure 7). This suggests that all simulation models are somewhat misspecified and our approach opens up various avenues to improve the models using explainable AI methods, such as SHAP values [see Figure 9 and Figure 10 in the Appendix 20, 21].

Model comparison After detecting model misspecification using the GEN score distribution, we have 55% in-distribution and 45% OOD SDSS data from stacking-MLP-RF-XGB classifier, 42% in-distribution and 58% OOD SDSS data from random forest and 71% in-distribution and 29% OOD SDSS data from XGBoost. Applying our BMC pipeline to the in-distribution dataset of the SDSS latent embeddings, we derive our final result shown in Figure 3. The bimodal shape results from the fact that the discarded OOD SDSS test data are primarily those classified between 40% and 60% as either NOAGN or TNG100, indicating that it is difficult for the classifier to make a definite prediction for them. There is a clear preference for the NOAGN model by all 3 classifiers considering the violin shape and the position of box-and-whisker plot inside each “violin” (see also Figure 8 in the Appendix). This relative preference does not necessarily mean that NOAGN fits the SDSS test set

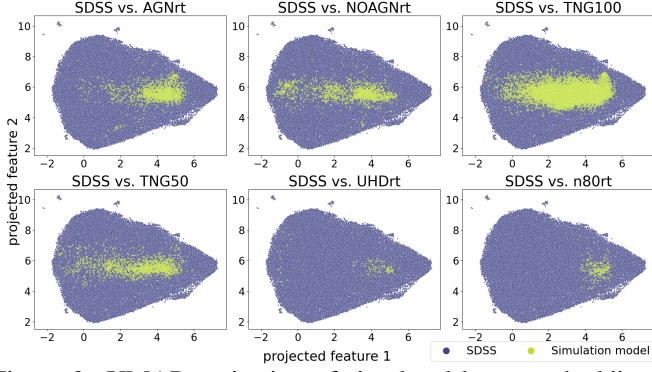


Figure 2: UMAP projection of simulated latent embeddings (yellow) compared to the SDSS test set (purple).

better than the other models. It simply points to the fact that, among all partly misspecified models (see above), NOAGN generates the most realistic images. But note that also a tiny fraction of the TNG100 and UHD galaxies are well in agreement with SDSS. Interestingly, comparing TNG100/TNG50 and NOAGN/UHD, we find that higher physical resolution does not necessarily provide better agreement with observations. This might reveal a mismatch between simulation resolution and the employed sub-grid physics which might fail to result in realistic simulations if not adapted for higher resolution.

Physical insights through SHAP values

We interpret our model comparison results qualitatively in light of physical difference between the simulation models via an analysis of SHAP values on the XGBoost classifier. The resulting SHAP plots are shown in Figure 4 below (full figure see Figure 9) and Figure 10 in the appendix and discussed in more depth there as well. This analysis suggests that NOAGN must be redder and clumpier than TNG100, which, in turn, must be bluer and smoother. This difference might point towards different star formation histories and present day star formation rates, since younger stars are on average bluer.

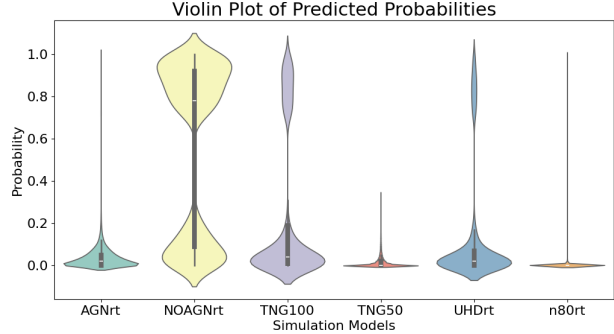


Figure 3: The violin plot for the stacking-MLP-RF-XGB classification of the in-distribution data of SDSS test set. It displays the distribution of predicted model probabilities $p(\mathcal{M} | \mathcal{D}_i)$ over all data \mathcal{D}_i (y-axis) for 6 simulation models (x-axis).

on average bluer.

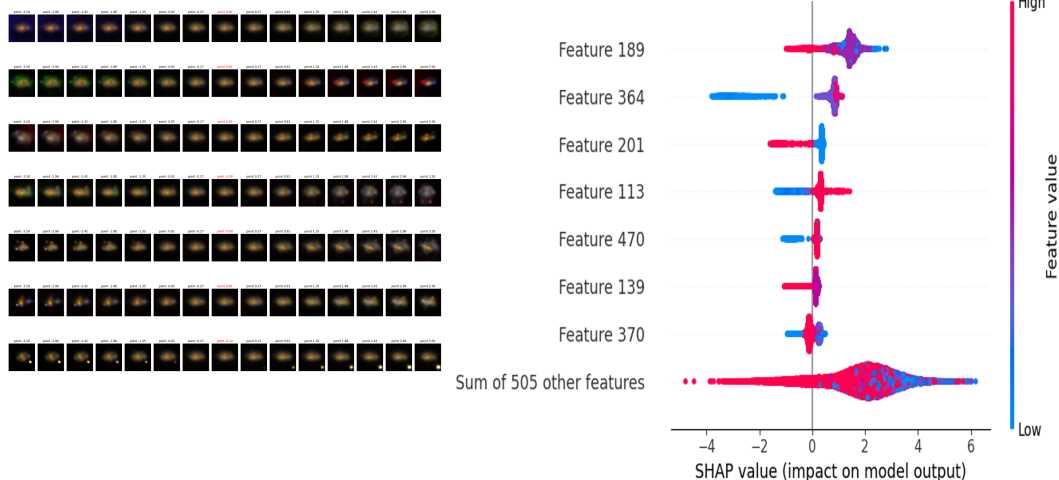


Figure 4: SHAP plot for NOAGN model from the XGBoost classifier. Feature n in the right panel corresponds to the n -th dimension of latent embeddings. To the left of the feature number we add corresponding visualisations of the latent dimensions. The middle column of the left small panels indicated by a red title shows the reconstruction from an encoded latent embedding of an example galaxy. To the left (right) we reduce (increase) the value of that entry in the latent embedding. We vary latent embedding entries by about 3σ around the mean in each dimension. For example, feature 189 shows strong colour variation while feature 470 shows strong structural variation.

5 Conclusion

We have explored novel approaches to model misspecification detection and Bayesian model comparison in the context of galaxy images and hydrodynamical simulations. Our approach for detecting model misspecification not only enables us to gauge the misfit of individual models, but also enables insights on why or in which respect these models are misspecified. By casting the Bayesian model comparison task as a classification task, we are able to select the relatively best matching model without the need for potentially lossy hand-crafted summary statistics. Furthermore our approach enables the use of explainable AI techniques, such as SHAP values, to obtain a deeper insight into the advantages and disadvantages of individual models.

Broader impact statement

The authors are not aware of any immediate ethical or societal implications of this work. This work purely aims to aid scientific research and proposes to apply novel Bayesian model comparison techniques in order to distinguish between different simulation models.

References

- [1] Samet Akcay, Amir Atapour-Abarghouei, and Toby P Breckon. Gandomaly: Semi-supervised anomaly detection via adversarial training. In *Computer Vision–ACCV 2018: 14th Asian Conference on Computer Vision, Perth, Australia, December 2–6, 2018, Revised Selected Papers, Part III 14*, pages 622–637. Springer, 2019.
- [2] Peter Behroozi, Risa H Wechsler, Andrew P Hearin, and Charlie Conroy. Universemachine: The correlation between galaxy growth and dark matter halo assembly from $z=0$ -10. *Monthly Notices of the Royal Astronomical Society*, 488(3):3143–3194, 2019.
- [3] Marvin Blank, Andrea V Macciò, Aaron A Dutton, and Aura Obreja. Nihao–xxii. introducing black hole formation, accretion, and feedback into the nihao simulation suite. *Monthly Notices of the Royal Astronomical Society*, 487(4):5476–5489, 2019.
- [4] Tobias Buck, Andrea V Macciò, Aaron A Dutton, Aura Obreja, and Jonas Frings. Nihao xv: the environmental impact of the host galaxy on galactic satellite and field dwarf galaxies. *Monthly Notices of the Royal Astronomical Society*, 483(1):1314–1341, 2019.
- [5] Tobias Buck, Aura Obreja, Andrea V Macciò, Ivan Minchev, Aaron A Dutton, and Jeremiah P Ostriker. Nihao-uhd: the properties of mw-like stellar discs in high-resolution cosmological simulations. *Monthly Notices of the Royal Astronomical Society*, 491(3):3461–3478, 2020.
- [6] Peter Camps and Maarten Baes. Skirt: An advanced dust radiative transfer code with a user-friendly architecture. *Astronomy and Computing*, 9:20–33, 2015.
- [7] F. J. Castander. The Sloan digital sky survey. *Astrophysics and Space Science*, 263:91–94, 1998. doi: 10.1023/A:1002196414003.
- [8] Tianqi Chen and Carlos Guestrin. Xgboost: A scalable tree boosting system. In *Proceedings of the 22nd ACM SIGKDD international conference on knowledge discovery and data mining*, pages 785–794, 2016.
- [9] Kyle Cranmer, Johann Brehmer, and Gilles Louppe. The frontier of simulation-based inference. *Proceedings of the National Academy of Sciences*, 117(48):30055–30062, 2020.
- [10] Lasse Elsemüller, Hans Olischläger, Marvin Schmitt, Paul-Christian Bürkner, Ullrich Köthe, and Stefan T Radev. Sensitivity-aware amortized bayesian inference. *arXiv preprint arXiv:2310.11122*, 2023.
- [11] Lasse Elsemüller, Martin Schnuerch, Paul-Christian Bürkner, and Stefan T. Radev. A deep learning method for comparing bayesian hierarchical models, 2023.
- [12] Tilmann Gneiting and Adrian E Raftery. Strictly proper scoring rules, prediction, and estimation. *Journal of the American Statistical Association*, 102(477):359–378, 2007.
- [13] Ian Goodfellow, Jean Pouget-Abadie, Mehdi Mirza, Bing Xu, David Warde-Farley, Sherjil Ozair, Aaron Courville, and Yoshua Bengio. Generative adversarial networks. *Communications of the ACM*, 63(11):139–144, 2020.
- [14] Zehao Jin, Andrea V Macciò, Nicholas Faucher, Mario Pasquato, Tobias Buck, Keri L Dixon, Nikhil Arora, Marvin Blank, and Pavle Vulanovic. Quantitatively rating galaxy simulations against real observations with anomaly detection. *Monthly Notices of the Royal Astronomical Society*, 529(4):3536–3549, 2024.
- [15] Konstantin Karchev, Roberto Trotta, and Christoph Weniger. Simsims: Simulation-based supernova ia model selection with thousands of latent variables. *arXiv preprint arXiv:2311.15650*, 2023.

- [16] Diederik P Kingma and Jimmy Ba. Adam: A method for stochastic optimization. *arXiv preprint arXiv:1412.6980*, 2014.
- [17] Diederik P Kingma and Max Welling. Auto-encoding variational bayes. *arXiv preprint arXiv:1312.6114*, 2013.
- [18] Juna Kollmeier, SF Anderson, GA Blanc, MR Blanton, KR Covey, J Crane, N Drory, PM Frinchaboy, CS Froning, JA Johnson, et al. Sdss-v pioneering panoptic spectroscopy. *Bulletin of the American Astronomical Society*, 2019.
- [19] Xixi Liu, Yaroslava Lochman, and Christopher Zach. Gen: Pushing the limits of softmax-based out-of-distribution detection. In *Proceedings of the IEEE/CVF Conference on Computer Vision and Pattern Recognition*, pages 23946–23955, 2023.
- [20] Scott M Lundberg and Su-In Lee. A unified approach to interpreting model predictions. *Advances in neural information processing systems*, 30, 2017.
- [21] Scott M Lundberg, Gabriel Erion, Hugh Chen, Alex DeGrave, Jordan M Prutkin, Bala Nair, Ronit Katz, Jonathan Himmelfarb, Nisha Bansal, and Su-In Lee. From local explanations to global understanding with explainable ai for trees. *Nature machine intelligence*, 2(1):56–67, 2020.
- [22] Robert Lupton, Michael R Blanton, George Fekete, David W Hogg, Wil O’Mullane, Alex Szalay, and Nicholas Wherry. Preparing red-green-blue images from ccd data. *Publications of the Astronomical Society of the Pacific*, 116(816):133, 2004.
- [23] Andrea V Macciò, Mohamad Ali-Dib, Pavle Vulanovic, Hind Al Noori, Fabian Walter, Nico Krieger, and Tobias Buck. Using artificial intelligence and real galaxy images to constrain parameters in galaxy formation simulations. *Monthly Notices of the Royal Astronomical Society*, 512(2):2135–2141, 2022.
- [24] David JC MacKay. *Information theory, inference and learning algorithms*. Cambridge university press, 2003.
- [25] Alireza Makhzani and Brendan Frey. K-sparse autoencoders. *arXiv preprint arXiv:1312.5663*, 2013.
- [26] Jean-Michel Marin, Pierre Pudlo, Arnaud Estoup, and Christian Robert. Likelihood-free model choice. In *Handbook of approximate Bayesian computation*, pages 153–178. Chapman and Hall/CRC, 2018.
- [27] Leland McInnes, John Healy, and James Melville. Umap: Uniform manifold approximation and projection for dimension reduction. *arXiv preprint arXiv:1802.03426*, 2018.
- [28] Alan Meert, Vinu Vikram, and Mariangela Bernardi. A catalogue of 2d photometric decompositions in the sdss-dr7 spectroscopic main galaxy sample: preferred models and systematics. *Monthly Notices of the Royal Astronomical Society*, 446(4):3943–3974, 2015.
- [29] Benjamin P Moster, Rachel S Somerville, Christian Maulbetsch, Frank C Van Den Bosch, Andrea V Macciò, Thorsten Naab, and Ludwig Oser. Constraints on the relationship between stellar mass and halo mass at low and high redshift. *The Astrophysical Journal*, 710(2):903, 2010.
- [30] Mahdi Pakdaman Naeini, Gregory Cooper, and Milos Hauskrecht. Obtaining well calibrated probabilities using bayesian binning. In *Proceedings of the AAAI conference on artificial intelligence*, volume 29, 2015.
- [31] Dylan Nelson, Annalisa Pillepich, Volker Springel, Rüdiger Pakmor, Rainer Weinberger, Shy Genel, Paul Torrey, Mark Vogelsberger, Federico Marinacci, and Lars Hernquist. First results from the tng50 simulation: galactic outflows driven by supernovae and black hole feedback. *Monthly Notices of the Royal Astronomical Society*, 490(3):3234–3261, 2019.

- [32] Dylan Nelson, Volker Springel, Annalisa Pillepich, Vicente Rodriguez-Gomez, Paul Torrey, Shy Genel, Mark Vogelsberger, Ruediger Pakmor, Federico Marinacci, Rainer Weinberger, et al. The *illustris*ng simulations: public data release. *Computational Astrophysics and Cosmology*, 6:1–29, 2019.
- [33] Annalisa Pillepich, Dylan Nelson, Lars Hernquist, Volker Springel, Rüdiger Pakmor, Paul Torrey, Rainer Weinberger, Shy Genel, Jill P Naiman, Federico Marinacci, et al. First results from the *illustris*ng simulations: the stellar mass content of groups and clusters of galaxies. *Monthly Notices of the Royal Astronomical Society*, 475(1):648–675, 2018.
- [34] Annalisa Pillepich, Volker Springel, Dylan Nelson, Shy Genel, Jill Naiman, Rüdiger Pakmor, Lars Hernquist, Paul Torrey, Mark Vogelsberger, Rainer Weinberger, et al. Simulating galaxy formation with the *illustris*ng model. *Monthly Notices of the Royal Astronomical Society*, 473(3):4077–4106, 2018.
- [35] Annalisa Pillepich, Dylan Nelson, Volker Springel, Rüdiger Pakmor, Paul Torrey, Rainer Weinberger, Mark Vogelsberger, Federico Marinacci, Shy Genel, Arjen van der Wel, et al. First results from the tng50 simulation: the evolution of stellar and gaseous discs across cosmic time. *Monthly Notices of the Royal Astronomical Society*, 490(3):3196–3233, 2019.
- [36] Pierre Pudlo, Jean-Michel Marin, Arnaud Estoup, Jean-Marie Cornuet, Mathieu Gautier, and Christian P Robert. Reliable abc model choice via random forests. *Bioinformatics*, 32(6):859–866, 2016.
- [37] Stefan T Radev, Marco D’Alessandro, Ulf K Mertens, Andreas Voss, Ullrich Köthe, and Paul-Christian Bürkner. Amortized bayesian model comparison with evidential deep learning. *IEEE Transactions on Neural Networks and Learning Systems*, 34(8):4903–4917, 2021.
- [38] Stefan T Radev, Marvin Schmitt, Lukas Schumacher, Lasse Elsemüller, Valentin Pratz, Yannik Schälte, Ullrich Köthe, and Paul-Christian Bürkner. Bayesflow: Amortized bayesian workflows with neural networks. *arXiv preprint arXiv:2306.16015*, 2023.
- [39] Christian P Robert, Jean-Marie Cornuet, Jean-Michel Marin, and Natesh S Pillai. Lack of confidence in approximate bayesian computation model choice. *Proceedings of the National Academy of Sciences*, 108(37):15112–15117, 2011.
- [40] Vicente Rodriguez-Gomez, Gregory F Snyder, Jennifer M Lotz, Dylan Nelson, Annalisa Pillepich, Volker Springel, Shy Genel, Rainer Weinberger, Sandro Tacchella, Rüdiger Pakmor, et al. The optical morphologies of galaxies in the *illustris*ng simulation: a comparison to pan-starrs observations. *Monthly Notices of the Royal Astronomical Society*, 483(3):4140–4159, 2019.
- [41] Marvin Schmitt, Paul-Christian Bürkner, Ullrich Köthe, and Stefan T Radev. Detecting model misspecification in amortized bayesian inference with neural networks. In *DAGM German Conference on Pattern Recognition*, pages 541–557. Springer, 2023.
- [42] Volker Springel, Rüdiger Pakmor, Annalisa Pillepich, Rainer Weinberger, Dylan Nelson, Lars Hernquist, Mark Vogelsberger, Shy Genel, Paul Torrey, Federico Marinacci, et al. First results from the *illustris*ng simulations: matter and galaxy clustering. *Monthly Notices of the Royal Astronomical Society*, 475(1):676–698, 2018.
- [43] R Brent Tully and J Richard Fisher. A new method of determining distances to galaxies. *Astronomy and Astrophysics*, vol. 54, no. 3, Feb. 1977, p. 661-673., 54:661–673, 1977.
- [44] Aäron Van Den Oord, Nal Kalchbrenner, and Koray Kavukcuoglu. Pixel recurrent neural networks. In *International conference on machine learning*, pages 1747–1756. PMLR, 2016.
- [45] Mark Vogelsberger, Shy Genel, Volker Springel, Paul Torrey, Debora Sijacki, Dandan Xu, Greg Snyder, Dylan Nelson, and Lars Hernquist. Introducing the *Illustris* project: simulating the coevolution of dark and visible matter in the universe. *Monthly Notices of the Royal Astronomical Society*, 444(2):1518–1547, 2014.
- [46] Mark Vogelsberger, Federico Marinacci, Paul Torrey, and Ewald Puchwein. Cosmological simulations of galaxy formation. *Nature Reviews Physics*, 2(1):42–66, 2020.

- [47] Liang Wang, Aaron A Dutton, Gregory S Stinson, Andrea V Macciò, Camilla Penzo, Xi Kang, Ben W Keller, and James Wadsley. Nihao project-i. reproducing the inefficiency of galaxy formation across cosmic time with a large sample of cosmological hydrodynamical simulations. *Monthly Notices of the Royal Astronomical Society*, 454(1):83–94, 2015.
- [48] Stefan Waterval, Sana Elgamal, Matteo Nori, Mario Pasquato, Andrea V Macciò, Marvin Blank, Keri L Dixon, Xi Kang, and Tengiz Ibrayev. Nihao–xxviii. collateral effects of agn on dark matter concentration and stellar kinematics. *Monthly Notices of the Royal Astronomical Society*, 514(4):5307–5319, 2022.
- [49] Jingkang Yang, Kaiyang Zhou, Yixuan Li, and Ziwei Liu. Generalized out-of-distribution detection: A survey. *International Journal of Computer Vision*, pages 1–28, 2024.
- [50] Lorenzo Zanisi, Marc Huertas-Company, Francois Lanusse, Connor Bottrell, Annalisa Pillepich, Dylan Nelson, Vicente Rodriguez-Gomez, Francesco Shankar, Lars Hernquist, Avishai Dekel, et al. A deep learning approach to test the small-scale galaxy morphology and its relationship with star formation activity in hydrodynamical simulations. *Monthly Notices of the Royal Astronomical Society*, 501(3):4359–4382, 2021.
- [51] Shengjia Zhao, Jiaming Song, and Stefano Ermon. Infvae: Information maximizing variational autoencoders. *arXiv preprint arXiv:1706.02262*, 2017.

A Appendix: Training of VAE and supplemental figures

For training the k -sparse VAE we use the Adam optimizer [16] with an initial learning rate of 10^{-3} and a reduce-on-plateau schedule for dynamically reducing the learning rate by a factor of 0.1 if the average validation loss per epoch has no improvement after 5 epochs. We have an early stopping mechanism in place, where the training halts if the average validation loss does not decrease for 10 consecutive epochs in which case we choose the model checkpoint at those previous 10 epochs. Using a batch size of 400, the training of the k -sparse VAE for 38 epochs on a single A100 GPU takes 6,802 seconds. The final model checkpoint which we evaluate is hence at the 28th epoch.

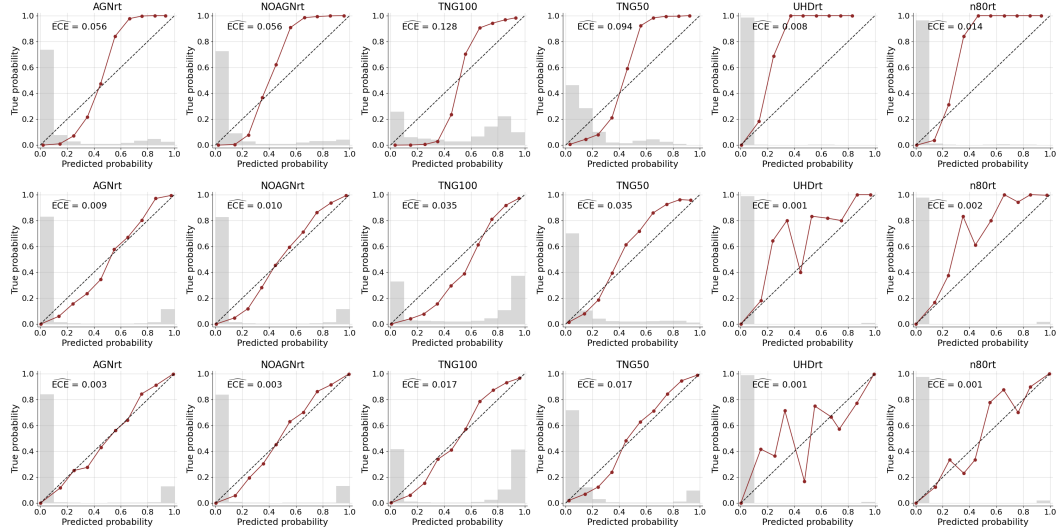


Figure 5: Calibration curves of classifiers. Top: random forest, Middle: XGBoost, Bottom: stacking-MLP-RF-XGB

B SHAP analysis

We qualitatively interpret our model comparison results in light of physical difference of the simulation models via an analysis of SHAP values on the XGBoost classifier. The resulting SHAP plots are

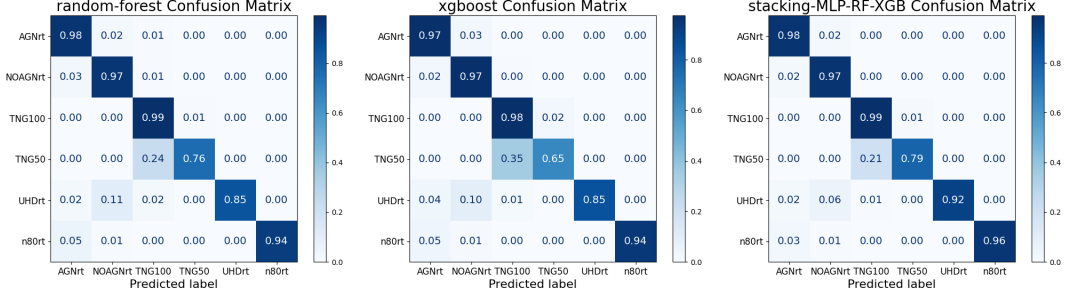


Figure 6: Confusion matrices of classifiers. Left: random forest, Middle: XGBoost, Right: stacking-MLP-RF-XGB

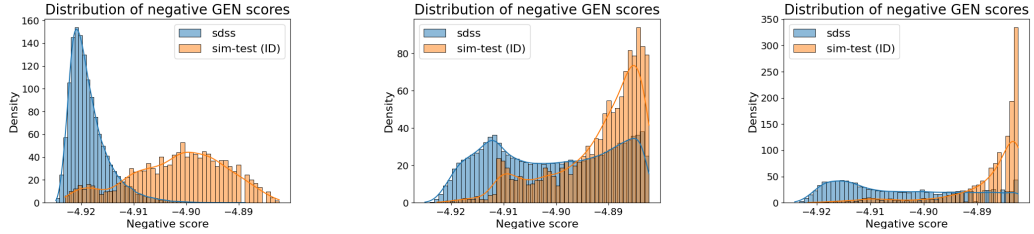


Figure 7: GEN score distribution of all simulation models test set (orange) and SDSS test set (blue). Left: random forest, Middle: XGBoost, Right: stacking-MLP-RF-XGB

shown in Figure 9 and Figure 10. Since feature dimensions are ordered by their importance on the prediction of the XGBoost classifier result the upper and lower panel have slightly different rankings and show different feature vectors. However, feature 364 and 189 are similarly important for NOAGN and TNG100 classification. Additionally the importance of feature 113 and 205 are also shared between the two models. We find that two features (189 and 364) in the compressed latent space are equally important for classifying NOAGN and TNG100. However, their effect on the classification output is exactly opposite - for NOAGN (TNG100) these features have an overall positive (negative) impact on the classification if they show a large feature value. Looking at the meaning of these two features, we find that 189 strongly correlates with color where a low feature value represents more red galaxies and a larger value encodes bluer ones. Similarly, feature 364 encode green to red galaxies where additionally the substructure inside the galaxy varies with feature value, the larger (smaller) this feature the more red (green) spots appear in the galaxies. From this we conclude that NOAGN must be redder and clumpier than TNG100 which must be bluer and smoother. This might point towards different star formation histories and present day star formation rates since younger stars are on average bluer. A similar conclusion can be drawn from the other two common features 205 and 113.

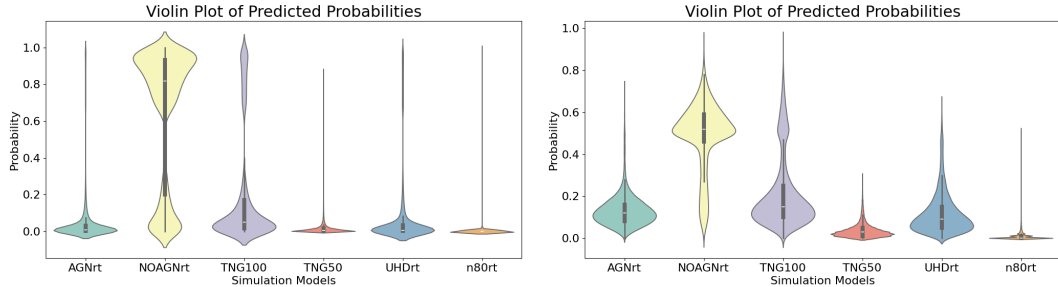


Figure 8: Violin plots showing the classification of the in-distribution data of SDSS test set for two other classifiers. Left: XGBoost, Right: random forest.

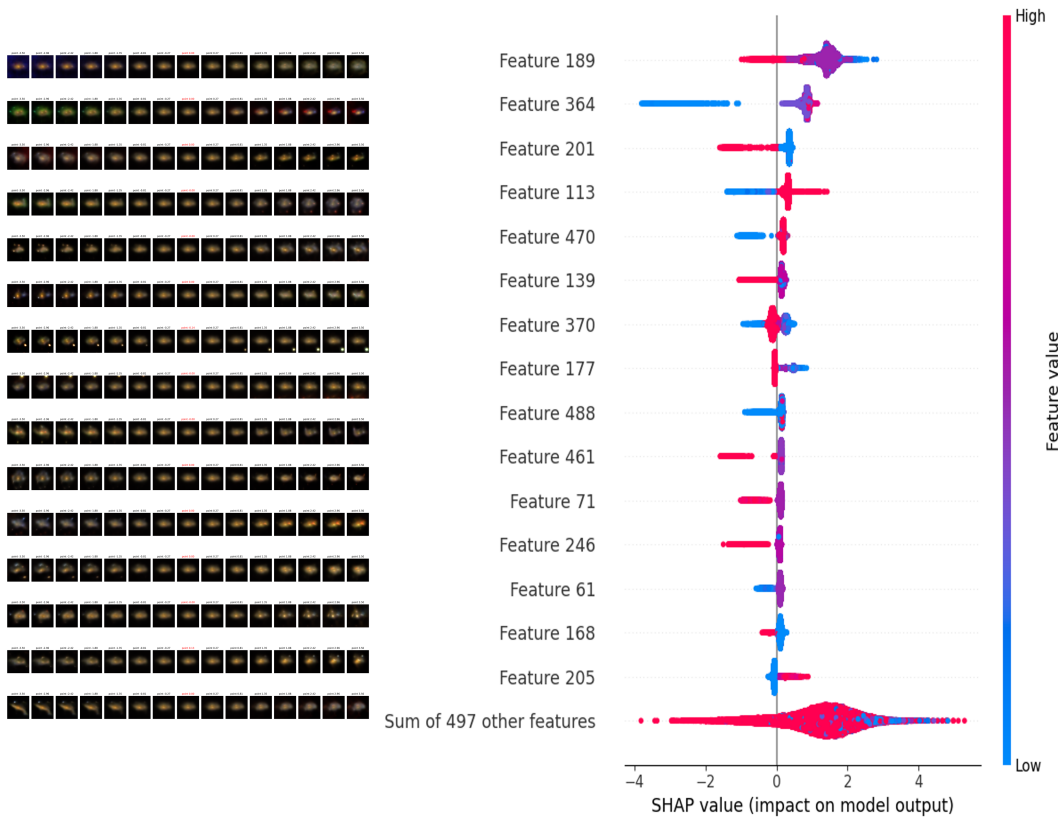


Figure 9: SHAP plot for NOAGN model from the XGBoost classifier (full figure)

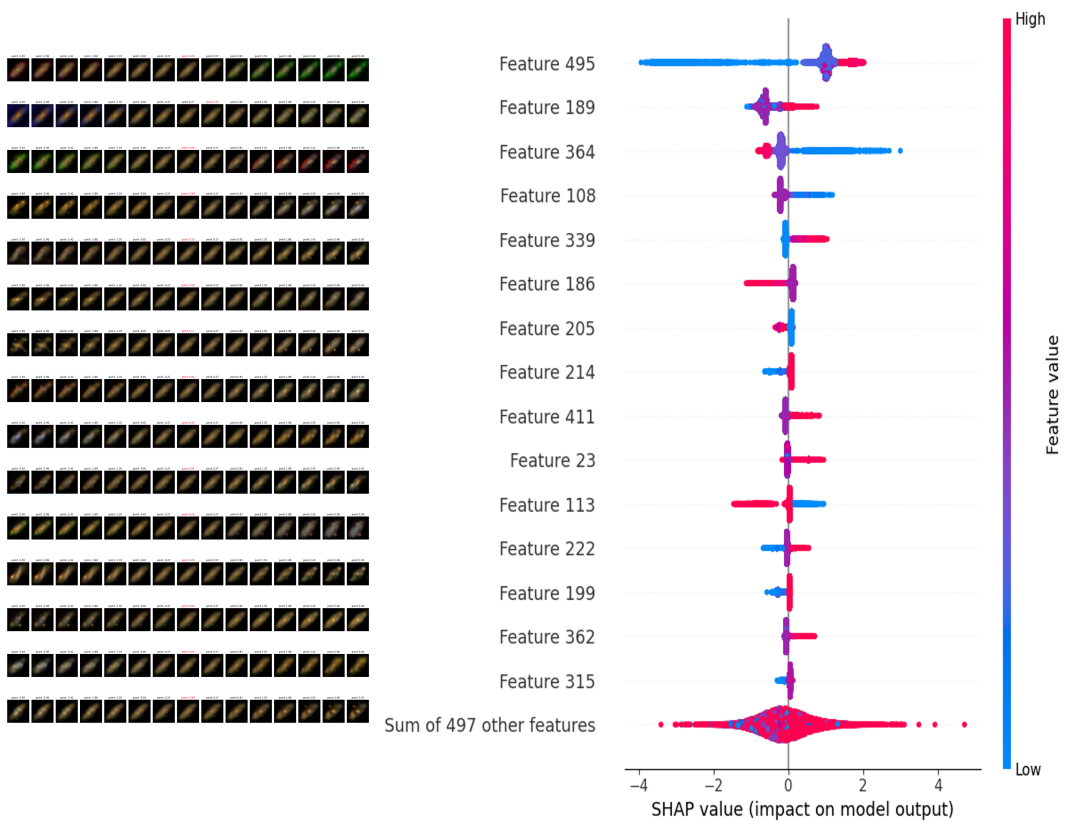


Figure 10: An example of SHAP plot for TNG100 from the XGBoost classifier. Features 495 shows strong colour variation while features 205 shows strong structural variation.